
Quantification of Glucose Transport and Phosphorylation in Human Skeletal Muscle Using FDG PET

Martin Reinhardt, Markus Beu, Henning Vosberg, Hans Herzog, Achim Hübinger, Hans Reinauer and Hans-Wilhelm Müller-Gärtner

Department of Nuclear Medicine, Heinrich-Heine-University, Düsseldorf; Forschungszentrum Juelich; and Diabetes Research Institute, Düsseldorf, Germany

PET with 2-[¹⁸F]-fluoro-2-deoxy-D-glucose (FDG) is used for quantifying glucose metabolism in brain and myocardium in vivo. We developed and validated a similar procedure for the quantification of the two initial steps of glucose metabolism in skeletal muscle in vivo. **Methods:** The measurement protocol was first optimized by computer simulations. In addition to the accuracy in sampling plasma input and tissue time-activity curves, precise determination of the fractional blood volume, that is, the extracellular tissue volume fraction, plays a key role in correctness of the determined model constants. The optimized protocol was subsequently used to estimate transmembrane muscular glucose transport and hexokinase activity in six human subjects with normal or altered glucose utilization. PET was performed during the steady state of an euglycemic hyperinsulinemic clamp. **Results:** A three-compartment model provides a better description of the experimental data than a two- or four-compartment model. Glucose clearance from the extracellular compartment into the skeletal muscle cell (K_1) ranges from 0.024 to 0.093 mL/g/min. The intracellular glucose phosphorylation rate (k_3) varies between 0.030 and 0.142 min⁻¹. The regional muscular glucose utilization, as calculated from the determined model parameters, lies between 10.7 and 83.3 μmol/kg/min and correlates with the whole-body glucose utilization as independently determined ($R^2 = 0.83$; $P \leq 0.01$). **Conclusion:** We demonstrate by computer simulations that a three-compartment model can be used to characterize the first two steps of glucose metabolism in skeletal muscle. An optimized measurement protocol is developed and applied to experimental data. This experimental approach should be appropriate to test whether glucose transport or hexokinase activity is altered in disorders of muscular glucose utilization.

Key Words: glucose metabolism; skeletal muscle; FDG PET; hexokinase; glucose transport; PET

J Nucl Med 1999; 40:977-985

Skeletal muscle is a major organ for glucose utilization and accounts for up to 85% of the whole-body glucose

utilization in healthy humans under insulin-stimulated conditions (1). This study develops and evaluates an experimental method to quantify the two initial steps of muscular glucose metabolism in vivo. These two steps can be quantitatively assessed by 2-[¹⁸F]-fluoro-2-deoxy-D-glucose (FDG). FDG is a radioactive glucose analog that is transported across the cell membrane into the muscle cell and phosphorylated intracellularly by the enzyme hexokinase to FDG-6-phosphate (FDG-6-P). FDG-6-P does not further participate in the cascade of glucose metabolism and accumulates inside the cell because intracellular glucose-6-phosphatase activity is low in brain and muscle (2). Measurement of tissue FDG accumulation by PET has therefore been used to quantify regional glucose metabolic rates in brain and heart (3,4).

A three-compartment model has been found to be appropriate to describe cerebral glucose transport and phosphorylation by FDG PET (2). The model is shown in Figure 1. It comprises one extracellular and two intracellular compartments. Four parameters characterize the exchange of FDG between the three compartments. K_1 (mL/g/min) describes the clearance of FDG from the extracellular compartment into the cell, and k_2 (min⁻¹) describes the transport rate of unphosphorylated FDG from the cell back to the extracellular compartment. The intracellular metabolism of FDG is characterized by the rate constants k_3 (min⁻¹) for phosphorylation to FDG-6-P and k_4 (min⁻¹) for dephosphorylation.

Here we test the validity of this three-compartment model of cerebral FDG metabolism for measurements of glucose transport and phosphorylation in human skeletal muscle. A measurement protocol is developed and optimized using computer simulations with particular reference to plasma input sampling and tissue sampling rates. The influence of the fractional volume of the tissue region on the correctness of the determined model parameters is investigated in detail. Noise is not considered in the simulations. The reason for the omission of noise is that the noise in the tissue data, that is, the major noise component, can hardly be estimated correctly because of its multiple causes, such as PET camera parameters, count statistics, image reconstruction and image

Received Jun. 6, 1998; revision accepted Jan. 4, 1999.
For correspondence or reprints contact: Martin Reinhardt, MD, Department of Nuclear Medicine, Heinrich-Heine-University, Moorenstr. 5, D-40225 Düsseldorf, Germany.

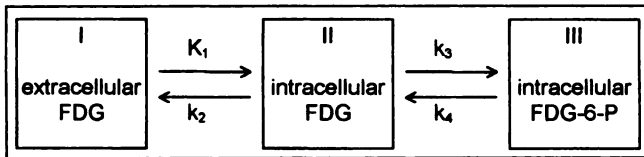


FIGURE 1. Three-compartment model of FDG metabolism.

filtering. Finally, experimental data from human subjects with normal or pathologic muscular glucose metabolism are used to demonstrate the plausibility of the model.

MATERIALS AND METHODS

Simulations

Generation of the Input Function and Tissue Data. The kinetic parameters of a compartment model are conventionally determined from the plasma input function and the tissue time-activity curve measured by PET (5).

As a first component of the simulations, we generated an input function and the corresponding tissue time-activity curve. On the basis of this generated data, we then determined the impact of variations in input and tissue sampling rates on the accuracy of the determined rate constants.

The input function G was generated using a multiexponential equation:

$$G(t) = [a_1(t - t_1) - a_2 - a_3]e^{-b_1(t-t_1)} + a_2e^{-b_2(t-t_1)} + a_3e^{-b_3(t-t_1)}. \quad \text{Eq. 1}$$

G is a function of the time t , which is characterized by a fast exponential decrease after the injection, due to diffusion of the tracer in the blood and two exponential terms describing the slow decrease caused by metabolism and excretion (6). G starts with the injection of the tracer and is calculated until 45 min postinjection. G is set to zero for times $t \leq t_1$, where t_1 expresses the time between the injection and the appearance of the tracer in the plasma samples. The parameters a_1 , a_2 , a_3 , b_1 , b_2 , b_3 and t_1 of G were defined according to a multiexponential fit of actually measured plasma input data from a healthy human subject (Table 1).

The tissue time-activity curve was calculated from G using a

TABLE 1
Parameters of Generated Input Function G and Generated Tissue Time-Activity Curve

Parameter	Value	Unit
t_1	0.467	min
a_1	377.40	kBq/mL/min
a_2	11.10	kBq/mL
a_3	3.70	kBq/mL
b_1	3.00	min ⁻¹
b_2	0.18	min ⁻¹
b_3	0.015	min ⁻¹
K_1	0.04	mL/g/min
k_2	0.15	min ⁻¹
k_3	0.09	min ⁻¹
k_4	0.00	min ⁻¹
FV	3.50	%

FV = fractional volume.

three-compartment model and previously reported values for K_1 , k_2 and k_3 determined in skeletal muscle tissue by FDG PET (7–9) (Table 1). The rate constant k_4 , indicating the dephosphorylation of FDG-6-P, was set to zero because it is negligible for times up to 45 min postinjection (8,10). The fractional volume (FV), which reflects the volume within the muscle tissue that contains extracellular but not intracellular tracer activity, was fixed to 3.5% as measured by PET with ¹⁵O-CO (11). The time t_0 describes the time difference between the appearance of the injection bolus in the sampled plasma input and the muscle tissue that is measured in the PET scanner. The time t_0 was set to 0.0 s in the simulations of the influences of input and tissue sampling and of FV.

Determination of the Compartment Model Parameters. The parameters K_1 , k_2 , k_3 , FV and t_0 were determined by nonlinear least square fits (5). All data points received the same statistical weight in the fitting procedure. The residual sum of squares (χ^2) reflecting the sum of the squared differences between the simulated and the fitted tissue time-activity curve was calculated from the fit data as a measure of fit quality (5).

Results of the Simulations. To investigate the influence of the input sampling on the determination of the model parameters, the time intervals between the samples of G were systematically prolonged. The input sampling schedules at a given sampling interval were selected in a way that the characterization of the bolus became as bad as possible (Fig. 2). The corresponding data are given in Table 2. These reduced sampling rates lead to incomplete descriptions of G during the bolus passage. As a consequence, the determined model parameters deviate from the correct values. Especially the parameters K_1 , k_2 , FV and t_0 show significant deviations from the correct values at sampling rates of one sample every 20 s or longer. At sampling rates up to one sample every 60 s, the quality of the determined model parameters is improved if parameter FV or t_0 is fixed to the predefined values of the simulations. If G is sampled every 120 s, the fit cannot be stabilized by fixing FV or t_0 . Sampling at rates of one sample every 15 s or faster leads to stable determinations of all model parameters with deviations below 5% compared with the correct values.

To determine the influence of the tissue sampling rate on the determination of the model parameters, we reduced the data points of the tissue time-activity curve during the initial 5 min of the study (Table 3). $G(t)$ was used for the determination of the model parameters. Sampling tissue data during the bolus transit at time frames of 120 s or longer leads to incorrect values for the parameters K_1 , k_2 and k_3 . The fit results can be stabilized by fixing the delay time t_0 or FV to the correct values. Tissue sampling with an initial frame duration up to 90 s gives stable and correct determinations of all parameters.

The influence of an incorrectly fixed FV or t_0 on the rate constants was simulated by fixing FV to values between 0% and 5% (Fig. 3) and by fixing t_0 to values from -30 to 40 s (Fig. 4). G and the continuous tissue time-activity curve were used for these simulations. These fit results and the values of χ^2 were compared with model fits with FV or t_0 fixed to the correct values. The simulations show the impact of an incorrectly predefined FV or t_0 on the model parameters. The parameters K_1 , k_2 and k_3 show significant deviations from the correct values; k_2 reacts the most sensitively to false values for FV and t_0 , with deviations up to 400% from the correct values. The best fit quality as documented by the lowest value for χ^2 is achieved with the correct values for FV and t_0 .

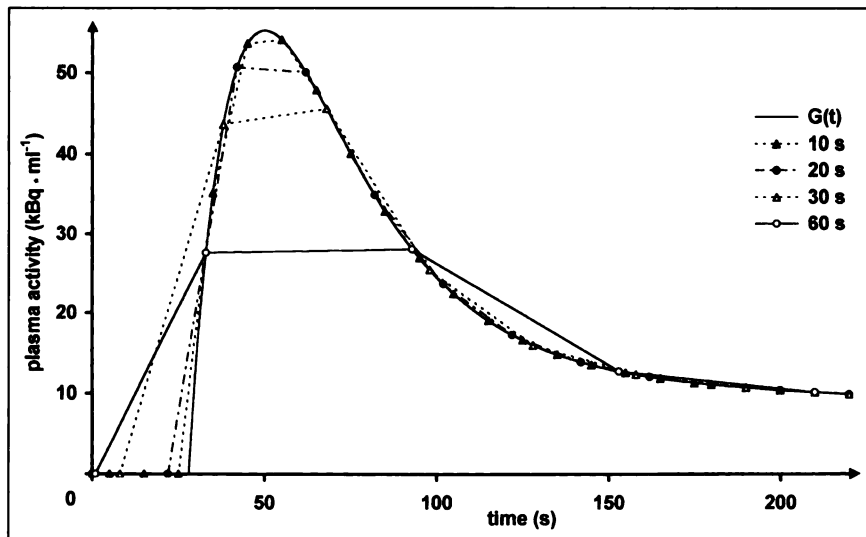


FIGURE 2. Generated input function $G(t)$ and input curves with reduced data sampling. Sampling input curve at intervals of 20 s or longer leads to incomplete characterization of bolus passage.

Experiments

Subjects. Six male human subjects with normal or pathologic glucose utilization were studied after an overnight fast. Three volunteers had type 2 diabetes (non-insulin-dependent diabetes mellitus [NIDDM]), 1 volunteer had been immobilized for 6 wk before the study as a result of severe coronary artery disease with cardiac decompensation and 2 volunteers were healthy (Table 4). Antidiabetic drugs and β -blockers were discontinued the day before the experiment. Patients under insulin substitution did not receive insulin on the day of the experiment. The study protocol was approved by the ethics commission of the Heinrich-Heine-University of Düsseldorf and by the local government regarding the radiation exposure. All subjects gave written informed consent before the examinations.

Euglycemic-Hyperinsulinemic Clamp. To achieve stable metabolic conditions during the PET measurements, the glucose metabolism was stabilized by an euglycemic-hyperinsulinemic clamp, referred to as the “clamp” (1). Insulin (Velasulin® Human; Novo Nordisk, Mainz, Germany) was infused intravenously at a constant rate (0.1 IU insulin/[kg body weight]/h). Glucose infusion was adjusted to blood glucose levels that were measured every 5 min to reach steady-state blood glucose levels of 80 mg/dL. The steady-state condition with stable blood glucose levels at constant glucose infusion rates was achieved 60–120 min after the start of the insulin infusion, depending on the glucose level of the volunteer after fasting. The whole-body glucose utilization (wbGU) was calculated from the average glucose infusion rate (GI) and the body

TABLE 2
Simulations: Influence of Input Sampling Interval on Fit Parameters K_1 , k_2 , k_3 , FV and t_0

Sampling interval	Fixed parameters	K_1 (mL/g/min)	SD	k_2 (min^{-1})	SD	k_3 (min^{-1})	SD	FV (%)	SD	t_0 (s)	SD	χ^2
G(t) continuous	—	0.040		0.150		0.090		3.50		0.0		0.004
5 s	—	0.040	<0.001	0.151	<0.001	0.090	<0.001	3.51	0.00	0.0	<0.01	0.003
10 s	—	0.039	<0.001	0.140	0.003	0.087	0.002	3.62	0.02	0.8	0.1	196.0
15 s	—	0.041	<0.001	0.155	0.002	0.090	0.001	3.64	0.01	-1.8	0.1	133.3
20 s	—	0.038	<0.001	0.129	0.005	0.083	0.003	3.77	0.03	1.7	0.2	612.6
20 s	FV	0.040	<0.001	0.156	0.005	0.093	0.003	3.50(f)		0.9	0.2	849.3
20 s	t_0	0.039	<0.001	0.146	0.006	0.090	0.004	3.57	0.03	0.0(f)		960.5
20 s	FV, t_0	0.040	<0.001	0.154	0.006	0.093	0.004	3.50(f)		0.0(f)		985.2
30 s	—	0.033	<0.001	0.093	0.011	0.073	0.009	4.15	0.09	8.9	0.5	4,226.2
30 s	FV	0.038	<0.001	0.150	0.014	0.097	0.009	3.50(f)		6.2	0.5	532.1
30 s	t_0	0.041	0.001	0.186	0.024	0.108	0.012	3.06	0.11	0.0(f)		961.0
30 s	FV, t_0	0.037	0.001	0.131	0.016	0.087	0.011	3.50(f)		0.0(f)		9,091.2
60 s	—	0.029	0.001	0.047	0.014	0.051	0.017	7.10	0.17	15.3	0.8	9,780.2
60 s	FV	2.210	13.820	0.442	0.028	0.393	0.022	3.50(f)		17.6	4.8	16,700.0
60 s	t_0	0.045	0.003	0.209	0.050	0.115	0.020	4.74	0.25	0.0(f)		18,818.0
60 s	FV, t_0	0.037	0.001	0.131	0.083	0.204	0.017	3.50(f)		0.0(f)		19,491.0
120 s	—	0.027	0.003	0.027	0.023	0.063	0.038	17.00	0.80	19.5	1.6	136.0
120 s	FV	12.00	82.00	75.00	511.00	0.109	0.008	3.50(f)		19.5	5.0	337.0
120 s	t_0	6.00	15.00	12.00	21.00	0.020	0.040	-58.00	125.00	0.0(f)		337.0
120 s	FV, t_0	0.420	0.150	2.400	1.000	0.100	0.010	3.50(f)		0.0(f)		829.0

FV = fractional volume; f = parameter fixed.

TABLE 3
 Simulations: Influence of Tissue Sampling Interval on Fit Parameters K_1 , k_2 , k_3 , FV and t_0

Sampling interval	Fixed parameters	K_1 (mL/g/min)	SD	k_2 (min ⁻¹)	SD	k_3 (min ⁻¹)	SD	FV (%)	SD	t_0 (s)	SD	χ^2
G(t) continuous	—	0.040		0.150		0.090		3.50		0.0		0.004
5 s	—	0.040	<0.001	0.150	<0.001	0.090	<0.001	3.50	<0.01	0.7	<0.01	0.003
10 s	—	0.040	<0.001	0.150	<0.001	0.090	<0.001	3.50	<0.01	0.0	<0.01	0.002
15 s	—	0.040	<0.001	0.150	<0.001	0.090	<0.001	3.50	<0.01	0.0	<0.01	0.002
20 s	—	0.040	<0.001	0.150	<0.001	0.090	<0.001	3.50	<0.01	0.0	<0.01	0.002
30 s	—	0.040	<0.001	0.150	<0.001	0.090	<0.001	3.50	<0.01	0.0	<0.01	0.002
60 s	—	0.040	<0.001	0.150	<0.001	0.090	<0.001	3.50	<0.01	0.0	0.10	0.002
90 s	—	0.040	<0.001	0.150	<0.001	0.090	<0.001	3.48	0.02	0.6	0.50	0.002
90 s	—	0.041	<0.001	0.161	0.002	0.925	<0.001	3.5(f)		37.1	0.20	0.434
90 s	—	0.040	<0.001	0.150	<0.001	0.090	<0.001	3.50	<0.01	0.0(f)		0.002
90 s	—	0.040	<0.001	0.150	<0.001	0.090	<0.001	3.5(f)		0.0(f)		0.002
120 s	—	0.039	<0.001	0.148	0.003	0.095	<0.001	4.49	0.21	45.2	1.30	0.092
120 s	FV	0.041	<0.001	0.158	0.001	0.092	<0.001	3.5(f)		33.6	0.20	0.162
120 s	t_0	0.040	<0.001	0.150	<0.001	0.090	<0.001	3.50	<0.01	0.0(f)		0.002
120 s	FV, t_0	0.040	<0.001	0.150	<0.001	0.090	<0.001	3.5(f)		0.0(f)		0.002
180 s	—	0.022	0.058	0.019	0.416	0.060	0.778	1.29	3.54	528.5	11.50	9930.800
180 s	FV	0.041	0.046	0.145	0.424	0.091	0.142	3.5(f)		502.1	101.00	9942.000
180 s	t_0	0.040	<0.001	0.150	<0.001	0.090	<0.001	3.44	0.06	0.0(f)		0.002
180 s	FV, t_0	0.040	<0.001	0.150	<0.001	0.090	<0.001	3.5(f)		0.0(f)		0.002
240 s	—	0.038	<0.001	0.140	0.004	0.096	0.002	5.14	0.53	27.1	9.00	0.002
240 s	FV	0.040	<0.001	0.150	<0.001	0.090	<0.001	3.5(f)		1.1	1.30	0.002
240 s	t_0	0.040	<0.001	0.151	<0.001	0.090	<0.001	3.42	0.09	0.0(f)		0.002
240 s	FV, t_0	0.040	<0.001	0.150	<0.001	0.090	<0.001	3.5(f)		0.0(f)		0.002
300 s	—	0.047	0.114	0.172	0.231	0.076	0.274	-1.16	100.28	-29.2	1307.30	0.084
300 s	FV	0.040	<0.001	0.150	<0.001	0.090	<0.001	3.5(f)		-1.6	1.70	0.002
300 s	t_0	0.040	<0.001	0.151	<0.001	0.090	<0.001	3.39	0.11	0.0(f)		0.002
300 s	FV, t_0	0.040	<0.001	0.150	<0.001	0.090	<0.001	3.5(f)		0.0(f)		0.002

FV = fractional volume; f = parameter fixed.

weight (BW) during the steady state of the clamp:

$$wbGU = GI \times BW^{-1} \quad \text{Eq. 2}$$

Blood for determination of serum glucose and insulin was drawn from an arterialized hand vein. Insulin levels were determined in

the fasting state before initialization of the clamp and every 30 min during the steady state (Table 4). After FDG PET, the insulin infusion was terminated, and the glucose infusion rate was increased twofold until the patients reached their baseline blood glucose level. Patients were released after an observation time of 60 min.

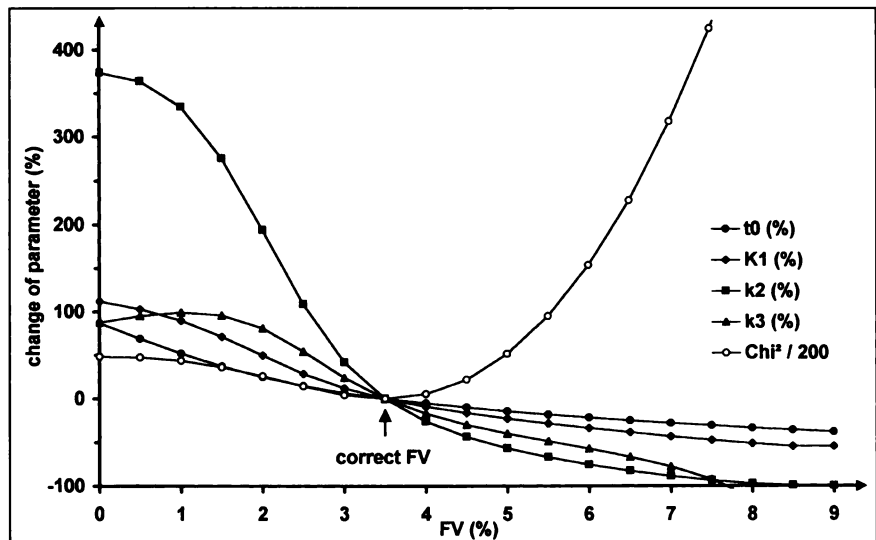


FIGURE 3. Simulation of influence of FV on fit. Parameters t_0 , K_1 , k_2 and k_3 show significant deviations from correct values if FV is fixed incorrectly. Increased values of χ^2 indicate reduced fit quality if FV is fixed to incorrect values.

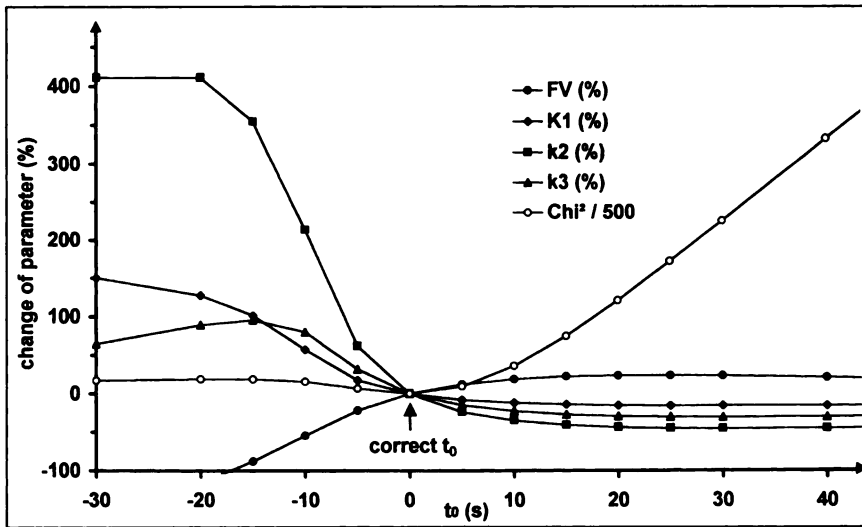


FIGURE 4. Simulation of influence of time delay t_0 on fit. Model parameters K_1 , k_2 , k_3 and FV show significant deviations from correct values if t_0 is fixed incorrectly. Increased values of χ^2 indicate reduced fit quality if t_0 is fixed to incorrect values.

PET. After the clamp had reached the steady state, the mid thigh region of the patient was positioned in the PET scanner (PET-Scanner, Type GE-4096 WB 7). Transmission data for attenuation correction were acquired by applying a ^{68}Ge -pin source (5×10^6 counts per slice).

FDG was synthesized according to the method described by Hamacher et al. (12) with a radiochemical purity > 98%. Intravenous injections of 370 MBq (10 mCi) FDG were administered at a constant rate within 10 s, followed by a flush of 20 mL physiologic saline. Dynamic measurement of emission data started with the injection of FDG. The dynamic protocol included 26 serial PET images within a total time of 45 min: 1×30 s, 12×5 s, 3×10 s, 4×30 s, 1×60 s and 8×300 s. The initial 30-s interval was chosen to skip the time delay between the intravenous injection and the appearance of the tracer in the femoral arteries. To allow determination of the input function, blood was sampled from an arterialized hand vein (every 6 s until 2 min postinjection, then every 30 s until 5 min postinjection and every 300 s until 45 min postinjection). The plasma (0.5 mL) was measured in a well counter to determine the input curve of FDG for the muscle tissue.

Images were reconstructed by filtered backprojection (Hanning filter, filter width 5 mm, correction for scatter and randoms) with a pixel size of 4×4 mm in a 128×128 matrix. Data for attenuation

correction were calculated from the transmission scans. A total of six regions of interest (ROIs) of the entire thigh muscle under exclusion of great vessels, bone and subcutaneous fat were defined in both thighs in three transversal slices (size of each ROI about 600 pixels or 60 mL). Time-activity analysis of the dynamic PET data was performed with decay-corrected data.

Fit of Rate Constants and Determination of Regional Glucose Transport and Regional Muscular Glucose Utilization. The rate constants K_1 , k_2 , k_3 and k_4 were determined with the sampled plasma input curve and the tissue time-activity curve from the PET measurement by a nonlinear least square fit as previously described. The rate constant k_4 (rate of intracellular dephosphorylation of glucose-6-phosphate [G-6-P]) was set to zero because the values for k_4 were smaller than the determined standard error of k_4 in all subjects.

The regional muscular glucose transport (rGT) was calculated from the transport constant K_1 and the plasma glucose level (G_{1p}), assuming identical affinities for FDG and glucose to the glucose transporter by:

$$\text{rGT} = K_1 \times G_{1p} \quad \text{Eq. 3}$$

The regional muscular glucose utilization (rGU) was determined from the model parameters and the G_{1p} , with the lumped constant

TABLE 4
Clinical Data and Parameters from Euglycemic Hyperinsulinemic Clamp

Subject no.	Age (y)	Body mass index (kg/m ²)	Diagnosis	Antidiabetic drugs (dose/d)	Plasma glucose fasting (mmol/L)	Plasma insulin fasting (μU/mL)	Plasma insulin steady state (μU/mL)
1	53	34.9	Healthy	None	5.44	11	79
2	40	28.9	Healthy	None	6.11	7	67
3	59	26.8	CAD, 6-wk immobilization	None	4.83	5	82
4	63	37.7	Type 2 diabetes for 9 y	Insulin 24 IU	6.67	12	76
5	48	30.9	Type 2 diabetes for 4 y	Acarbose 50 mg	8.94	11	93
6	58	31.3	Type 2 diabetes for 27 y	Insulin 41 IU	9.39	9	78

CAD = coronary artery disease.

(LC) assumed to be 1.0 in muscle tissue (13) by:

$$rGU = \frac{K_1 \times k_3}{k_2 + k_3} \times Gl_p \times LC^{-1}. \quad \text{Eq. 4}$$

The rGU is in accordance with the amount of glucose that is phosphorylated intracellularly by the hexokinase.

Statistical Analysis

The compartment model fits were tested by the Akaike information criterion (14), the Schwarz criterion (15) and the F statistic (16). These test criteria are calculated from the χ^2 values of the fits and include recognition of the number of compartments, fitted parameters and data points.

The determined regional muscular glucose utilization was correlated with the whole-body glucose utilization as measured during the steady state of the clamp. Significance of the regression between regional muscular and whole-body glucose utilization was tested by the Student *t* test.

Validity of the Three-Compartment Model

To test the correctness of the three-compartment model of FDG metabolism for skeletal muscle, additional parameter fits, applying models with two or four compartments, were conducted in the six studied subjects. The consideration of these compartment models is caused by the following arguments: It is possible that FDG is transported only from the extracellular compartment into the skeletal muscle cell (K_1) and back (k_2) but is not metabolized inside the muscle cell (as known for 3-o-methyl-glucose). On the other hand, the transport step across the cell membrane or the phosphorylation could be so fast that it cannot be mathematically isolated. These situations are correctly described by a model with two compartments. The model with an additional third tissue compartment (a total of four compartments) is tested because of the possibility of a different biochemical behavior of FDG in muscle tissue, for example, a further metabolization of FDG-6-P within the muscle cell or additional intermediate transport steps caused by a delayed transport from the blood vessel into the intercellular space. The four-compartment model includes two additional rate constants compared with the three-compartment model. If the two-compartment model or the four-compartment model describes the muscular FDG metabolism better, then fits that apply these models

should lead to superior fit qualities when compared with the three-compartment model.

In five of the six subjects, the Akaike information criterion, the Schwarz criterion and the F statistic show a significant superiority of the three-compartment model compared with the model with two compartments. In one subject, all three test approaches showed no significant results, but there was a trend toward the superiority of the three-compartment model (Table 5).

With a four-compartment model assumed, a unique fit solution could not be found in any of the six subjects. It was not possible to isolate mathematically a fourth compartment from the other three compartments. This mathematical interdependence between two compartments in all datasets indicates that muscular FDG metabolism is not described better by the four-compartment model compared with the three-compartment model.

RESULTS

The results of the compartment fits in the six studied subjects are given in Table 6. Values for the glucose transport from the extracellular compartment into the cell (K_1) range from 0.024 to 0.093 mL/g/min. The rate constant for the transport from the cell back to the blood vessel (k_2) is in the range between 0.045 and 0.81 min⁻¹; the intracellular phosphorylation rate (k_3) ranges from 0.030 to 0.142 min⁻¹. The regional metabolic rate constant (K_{MRGI}) and the regional muscular glucose utilization as calculated from the determined model parameters show a significant linear correlation ($R^2 = 0.83$, $P \leq 0.01$) (Table 7 and Fig. 5).

DISCUSSION

The data presented show by means of computer simulations and experiments that the initial two steps of muscular glucose metabolism, namely, the glucose transport and the intracellular phosphorylation, can be quantified with FDG PET using a three-compartment model.

Our simulations show, in concordance with a previous study, that insufficient determination of the plasma input and tissue time-activity curves leads to incorrect values for all

TABLE 5
Tests for Fit Quality of Six Studied Subjects Applying Two- and Three-Compartment Models

Subject no.	Test criterion	Three-compartment model	Two-compartment model	Difference	Relative change (+%)	F test
1	Akaike	133.4	180.6	47.2	35.4	78.5; $P < 0.05$
	Schwarz	139.6	190.9	51.3	36.7	
2	Akaike	220.7	222.1	1.4	0.6	2.4; $P > 0.05$
	Schwarz	229.1	234.5	5.4	2.4	
3	Akaike	67.7	95.6	27.9	41.2	14.0; $P < 0.05$
	Schwarz	72.7	104.6	31.9	43.9	
4	Akaike	144.7	240.5	95.8	66.2	156.5; $P < 0.05$
	Schwarz	152.0	251.9	99.9	65.7	
5	Akaike	60.0	79.4	19.4	32.3	12.7; $P < 0.05$
	Schwarz	64.6	88.1	23.5	36.4	
6	Akaike	247.3	349.3	102.0	41.2	524.9; $P < 0.05$
	Schwarz	255.3	359.2	103.9	40.7	

TABLE 6
Fit Results of Six Studied Subjects

Subject no.	K_1 (mL/g/min)	k_2 (min ⁻¹)	k_3 (min ⁻¹)	FV (%)	t_0 (s)
1	0.048 ± 0.011	0.38 ± 0.15	0.091 ± 0.020	0.9 ± 0.7	-12.9 ± 8.0
2	0.046 ± 0.015	0.21 ± 0.13	0.127 ± 0.023	5.4 ± 1.7	0.0 ± 5.7
3	0.035 ± 0.005	0.12 ± 0.02	0.030 ± 0.005	1.2 ± 0.3	-17.5 ± 3.8
4	0.093 ± 0.003	0.81 ± 0.08	0.142 ± 0.026	0.4 ± 0.4	-0.2 ± 2.6
5	0.033 ± 0.002	0.05 ± 0.02	0.064 ± 0.013	2.5 ± 0.2	-3.1 ± 0.5
6	0.024 ± 0.002	0.38 ± 0.02	0.047 ± 0.003	0.8 ± 0.3	-22.9 ± 5.9

Data are fit result ± SD.

model parameters (5). In our simulations, the model parameters are incorrectly determined at input sampling intervals longer than 15 s. The duration of the initial tissue sampling interval can be significantly longer; intervals up to 90 s lead to correct fits of the simulated data. The influence of FV on the model parameters and the impact of using fixed values for FV or t_0 to stabilize the fit have not been reported previously. Fixing FV or t_0 to incorrect values seriously influences the model parameters, as shown by our simulations. In the six studied subjects, FV ranges from 0.4% to 5.4% and t_0 from -22.9 to 0.0 s. As a consequence, FV and t_0 are parameters that cannot be fixed before the model fit because the correct values are unknown and have to be determined individually. An alternative way is measuring the regional muscular FV under clamp conditions by ¹⁵O-CO-PET (11).

A comparison of the statistical validity of fits in models with two, three and four compartments shows that the three-compartment model gives the best description of the FDG metabolism in the skeletal muscle and should be applied for quantification of muscular glucose metabolism. The stable fit results in all studied subjects and the significant correlation between regional muscular glucose utilization and whole-body glucose utilization provide further evidence that the three-compartment model is adequate for the description of muscular FDG metabolism. This three-compartment model has been established and validated for

quantification of the rate constants of glucose transport and glucose phosphorylation in the brain (2). It is applied in tumor tissue (17) and skeletal muscle tissue (8,9), but its validity has not been tested for skeletal muscle.

In all six studied subjects, the determined muscular model constants K_1 , k_2 and k_3 and the glucose metabolic rate K_{MRGI} were in the range of muscular values presented by Kelley et al. (8) for healthy and diabetic volunteers. Kelley et al. (8) determined the model constants in skeletal muscle during an euglycemic hyperinsulinemic clamp as well as in the fasting state. They found significant increases in k_3 and regional muscular glucose utilization at insulin stimulation in all studied subgroups (diabetic, lean nondiabetic and obese nondiabetic) and increased values for K_1 under insulin stimulation only in the lean nondiabetic subgroup. In the other two subgroups, no significant effect of insulin on K_1 was observed. Under insulin stimulation in all subgroups, k_2 remained unchanged. Kelley et al. (8) also found a significant correlation between muscular glucose utilization and whole-body glucose utilization. Selberg et al. (9) presented similar values in the skeletal muscle of healthy persons during clamp conditions for K_1 and the regional glucose utilization, but k_2 and k_3 were clearly lower. In both studies, FV and the delay time t_0 are not mentioned. It is possible that the omission of these parameters in the study by Selberg et al. (9) caused the differences in our results as well as those of Kelley et al. (8). Hawkins et al. (16) showed that the disregard of FV leads to significant differences in the rate constants in the brain.

Because the fitted parameters are in good concordance in all six tissue ROIs in every subject, noise is not a major problem in the proposed measurement protocol. Nevertheless, the longest frame duration that allows stable fits should be selected to minimize statistical noise.

Compared with FDG PET studies of the brain, the muscular parameters K_1 , k_2 and k_3 are in the same range (16). Quantification of regional glucose utilization in the myocardium by FDG PET revealed values (842.8 ± 91.1 $\mu\text{mol/kg/min}$) that were tenfold higher than in the femoral muscle (83.9 ± 10 $\mu\text{mol/kg/min}$) (18). In our data, regional muscular glucose utilization ranges between 10.7 and 83.3

TABLE 7
Results of Six Studied Subjects

Subject no.	Regional muscular glucose transport ($\mu\text{mol/kg/min}$)	Regional muscular glucose utilization ($\mu\text{mol/kg/min}$)	Whole-body glucose utilization ($\mu\text{mol/kg/min}$)
1	218.7	41.7	21.8
2	220.7	83.3	32.9
3	150.8	29.9	10.1
4	355.4	53.2	25.1
5	144.8	78.7	24.4
6	97.2	10.7	9.2

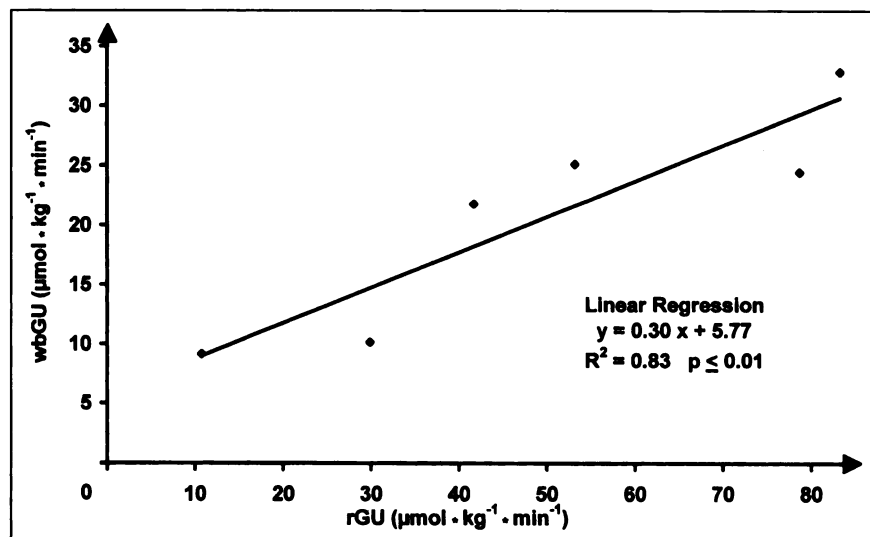


FIGURE 5. Linear regression between rGU and wbGU as reported in Table 7.

$\mu\text{mol}/\text{kg}/\text{min}$. The differences in the glucose utilization of skeletal muscle can be explained by the different degree of insulin stimulation, dissimilar glucose metabolism in white and red muscle fibers and individual parameters of the studied subjects, such as insulin resistance, age and body mass index in this study.

CONCLUSION

The data presented support the validity of the FDG model for determinations of glucose transport and phosphorylation in skeletal muscle. It is planned to apply the model for quantification of muscular glucose transport and phosphorylation in more patients with NIDDM or others with reduced glucose tolerance. Patients with NIDDM develop a muscular insulin resistance that is characterized by reduced muscular glucose utilization in general and a reduction of glycogen synthesis in particular (19). Similarly, the concentration of G-6-P, an intermediate of the intracellular glucose metabolism, is reduced (20). Several hypotheses may explain these findings: (a) The transport of glucose across the cellular membrane is impaired; (b) the intracellular phosphorylation of glucose to G-6-P is reduced; and (c) the degradation of G-6-P through the glycolysis and/or pentose phosphate pathway is increased. Kelley et al. (8) showed that the intracellular muscular glucose phosphorylation rate (k_3) and the regional muscular glucose utilization are reduced in patients with NIDDM, whereas the glucose transport constant (K_1) is not altered significantly compared with obese nondiabetic subjects. Further FDG PET studies shall provide more data on glucose transport and phosphorylation in insulin-resistant subjects.

ACKNOWLEDGMENT

This study was supported by a grant from the Deutsche Forschungsgemeinschaft (DFG), project B3 of Sonderforschungsbereich 351.

REFERENCES

- DeFronzo RA, Gunnarsson R, Björkman O, Olsson M, Wahren J. Effects of insulin on peripheral and splanchnic glucose metabolism in non-insulin-dependent (type II) diabetes mellitus. *J Clin Invest.* 1985;76:149-155.
- Phelps ME, Huang, SC, Hoffmann EJ, Selin C, Sokoloff L, Kuhl DE. Tomographic measurement of local cerebral glucose metabolic rate in humans with (F-18)2-fluoro-2-deoxy-D-glucose: validation of method. *Ann Neurol.* 1979;6:371-388.
- Mazziotta JC, Phelps ME. Positron emission tomography studies of the brain. In: Phelps M, Mazziotta J, Schelbert H, eds. *Positron Emission Tomography and Autoradiography: Principles and Applications for the Brain and Heart.* New York, NY: Raven; 1986:493-579.
- Schelbert HR, Schwaiger M. PET studies of the heart. In: Phelps M, Mazziotta J, Schelbert H, eds. *Positron Emission Tomography and Autoradiography: Principles and Applications for the Brain and Heart.* New York, NY: Raven; 1986:581-661.
- Mazoyer BM, Huesman RH, Budinger TF, Knittel BL. Dynamic PET data analysis. *J Comput Assist Tomogr.* 1986;10:645-653.
- Feng D, Wang X, Yan H. A computer simulation on the input function sampling schedules in tracer kinetic modeling with positron emission tomography (PET). *Comput Methods Programs Biomed.* 1994;45:175-186.
- Frey LD, Locher JTh, Hrycaj P, et al. Bestimmung der regionalen Glukose-Metabolisierungsrate der Lumbalmuskulatur bei Patienten mit generalisierter Tendomyopathie (GTM) mittels dynamischer ^{18}F -FDG-PET. *Z Rheumatol.* 1992; 51:238-242.
- Kelley DE, Mintun MA, Watkins SC, et al. The effect of non-insulin-dependent diabetes mellitus and obesity on glucose transport and phosphorylation in skeletal muscle. *J Clin Invest.* 1996;97:2705-2713.
- Selberg O, Burchert W, van den Hoff J, et al. Insulin resistance in liver cirrhosis. *J Clin Invest.* 1993;91:1897-1902.
- Lucignani G, Schmidt KC, Moresco RM, et al. Measurement of regional cerebral glucose utilization with fluorine-18-FDG and PET in heterogeneous tissues. *J Nucl Med.* 1993;34:360-369.
- Raitakari M, Knuuti MJ, Ruotsalainen U, et al. Insulin increases blood volume in human skeletal muscle: studies using ^{15}O]CO and positron emission tomography. *Am J Physiol.* 1995;269:E1000-E1005.
- Hamacher K, Coenen HH, Stöcklin G. Efficient stereospecific synthesis of no-carrier-added 2- ^{18}F fluoro-2-deoxy-D-glucose using aminopolyether supported nucleophilic substitution. *J Nucl Med.* 1986;27:235-238.
- Voipio-Pulkki L-M, Nuutila P, Knuuti MJ, et al. Heart and skeletal muscle glucose disposal in type 2 diabetic patients as determined by positron emission tomography. *J Nucl Med.* 1993;34:2064-2067.
- Akaike H. A new look at the statistical model identification. *IEEE Trans Automat Contr.* 1974;AC-19:716-723.
- Schwarz G. Estimating the dimension of a model. *Ann Stat.* 1978;6:461-564.

16. Hawkins RA, Phelps ME, Sung-Cheng H. Effects of temporal sampling, glucose metabolic rates, and disruption of the blood-brain barrier on the FDG model with and without a vascular compartment: studies in human brain tumors with PET. *J Cereb Blood Flow Metab.* 1986;6:170-183.
17. Wu H-M, Huang S-C, Choi Y, Hoh CK, Hawkins RA. A modeling method to improve quantitation of fluorodeoxyglucose uptake in heterogeneous tumor tissue. *J Nucl Med.* 1995;36:297-306.
18. Nuutila P, Knuuti MJ, Heinonen OJ, et al. Different alterations in the insulin stimulated glucose uptake in the athlete's heart and skeletal muscle. *J Clin Invest.* 1994;93:2267-2274.
19. Shulman GI, Rothman DL, Jue T, Stein P, DeFronzo RA, Shulman RG. Quantitation of muscle glycogen synthesis in normal subjects and subjects with non-insulin-dependent diabetes by ¹³C nuclear magnetic resonance spectroscopy. *N Engl J Med.* 1990;322:223-228.
20. Rothman DL, Shulman RG, Shulman GI. ³¹P nuclear magnetic resonance measurements of muscle glucose-6-phosphate. *J Clin Invest.* 1993;89:1069-1075.